Dyes and Pigments 120 (2015) 228–238

Contents lists available at ScienceDirect

Dyes and Pigments

journal homepage: www.elsevier.com/locate/dyepig

Porphyrin-vancomycin: A highly promising conjugate for the identification and photodynamic inactivation of antibiotic resistant Gram-positive pathogens

Le Zhai [1], Ke-Wu Yang [*, 1]

Key Laboratory of Synthetic and Natural Functional Molecule Chemistry of the Ministry of Education, College of Chemistry and Materials Science, Northwest University, Xi'an 710127, PR China

ARTICLE INFO

Article history:
Received 7 January 2015
Received in revised form
3 April 2015
Accepted 10 April 2015
Available online 24 April 2015

Keywords:
Antibiotic resistance
Vancomycin
Porphyrin
Photoinactivation
Photosensitizer
Surface plasmon resonance

ABSTRACT

The emergence of drug-resistant pathogens is a global public health problem. With the increasing antibiotic resistance of bacteria, there is an obvious need for the development for alternative therapeutics and materials that can effectively control this situation. In this work, a new conjugate, 5,10,15,20-tetrakis (*para*-aminophenyl) porphyrin-vancomycin was successfully explored for the identification and photoinactivation of antibiotic resistant Gram-positive pathogens. The minimum inhibitory concentration assay and photodynamic inactivation evaluation results revealed that the conjugate can effective inhibit the growth of 6 tested pathogenic strains under white light. The interaction intensity of the conjugate with Gram-positive and Gram-negative bacterial cells was evaluated by surface plasmon resonance, and the results showed that its activity toward *Staphylococcus aureus* was 14-fold larger than its activity toward *Escherichia coli* at 20 mM, indicating the conjugate selectively gathers in Gram-positive cells.

1. Introduction

Vancomycin (Van), an effective glycopeptide antibiotic used to treat β-lactam-resistant infections, was at one time believed to be the ultimate solution to defend human health [1–3]. However, because of its prevalent use for the treatments of common clinical infections, Van-resistant bacteria, such as vancomycin-resistant *Enterococcus faecium* (VRE) strains, emerged as a serious threat to public health [4–7]. A typical mechanism of Van resistance is mutation of the pathogen peptidoglycan sequence from D-Ala-D-Ala to D-Ala-D-Lac, resulting in a significant decrease of the binding affinity to Van molecules [8]. Recent studies expounded the detailed structure and activity of Van toward the cell wall peptide analogues of drug resistant bacteria [9], and also noted that merely increasing the binding affinity of Van to the D-Ala-D-Lac peptide precursors might not lead to a substantial improvement of the minimum inhibitory concentration (MIC) value against these pathogens [10,11]. Thus, the development of new antibacterial agents and alternative therapeutics to treat Van-resistant bacterial infections are imperative. Photodynamic antimicrobial chemotherapy (PACT) is one of the most promising antimicrobial regimens to control such situation [12]. In the PACT process, photosensitizers (PS) are irradiated with a specific wavelength of light and excited from the S_0 ground state to the S_1 excited state. Useful PS undergo intersystem crossing to the triplet excited state T_1 and transfer energy to triplet oxygen ($^3O_2$), converting it to singlet oxygen ($^1O_2$) (Fig. 1). The reactive oxygen species ($^1O_2$) are cytotoxic and can destroy the cell walls and membranes, resulting in cell death [13–15]. This approach to inactivate bacteria is unlikely to develop resistance to the photodynamic action of active oxygen species [16]. To date, PACT has been demonstrated effective in fighting against a variety of pathogens [17]. Nevertheless, the structure of fine PS towards antibiotic resistant bacteria is usually complicated, and it requires tedious manipulation to be achieved [18]. The most serious disadvantage of common PS is the lack of specificity [19–22], which renders PS molecules taken up by host cells improperly in the beginning of the PACT approach. Therefore, it is desirable to deliver PS molecules to the targeted pathogenic cells and avoid causing damage to the healthy cells by subsequent irradiation.

* Corresponding author. Tel./fax: +86 29 8153 5035.
E-mail address: kwyang@nwu.edu.cn (K.-W. Yang).
[1] Co-first author and contributed equally to this work.

http://dx.doi.org/10.1016/j.dyepig.2015.04.017
0143-7208/

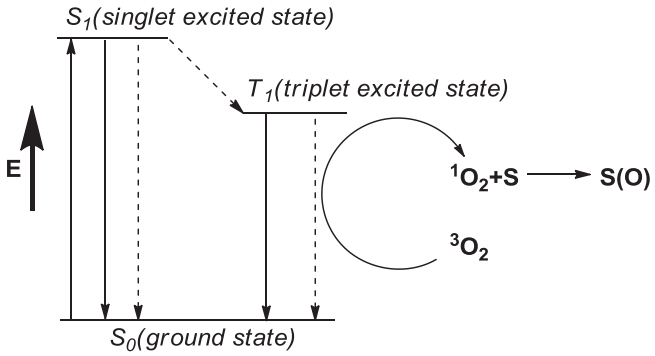

Fig. 1. Energy transduction in PACT process.

Porphyrins play significant roles in the field of photosynthesis and the Forster Resonance Energy Transfer (FRET) process [23]. Modified porphyrins at the *meso*-position exhibit valuable properties in biomedical applications involving photodiagnosis and cancer therapy [13,15] and are predominantly used in PACT [20,24]. Porphyrins are useful PS, whereas Van has specific binding affinity to the C-terminal L-Lys-D-Ala-D-Ala motif present in the cell wall of Gram-positive bacteria [3]. To effectively identify and kill the antibiotic resistant Gram-positive pathogens, our strategy is to construct the porphyrin-vancomycin conjugate, in which a vancomycin molecule is linked to the *meso*-position of 5,10,15,20-tetrakis (*para*-aminophenyl) porphyrin. Hence, PS molecules are led to the targeted cells by Van, causing destruction of the pathogenic cells under a specific wavelength of light irradiation. Based on this idea, the novel conjugate shown in Fig. 2 has been constructed.

2. Experiments

2.1. Materials and instruments

General chemicals were purchased from Sigma–Aldrich and were used without further purification. *Staphylococcus aureus* (ATCC 25923), *Escherichia coli* (ATCC 8739), *Enterococcus faecalis* (ATCC 51299), and *Bacillus subtilis* (ATCC 6633) cells were purchased from the Microbiology Institute of Shaanxi, China. Methicillin-resistant *S. aureus*-1 (MRSA-1), methicillin-resistant *S. aureus*-2 (MRSA-2), and VRE cells were collected at Xijing Hospital, Fourth Military Medical University, China. Luria–Bertani (LB) medium and Mueller–Hinton (MH) broth were used as the growth media for bacterial strains and were obtained from OXOID.

NMR spectra were recorded on an INOVA400 instrument (Varian, U.S.A.) at 400 MHz for ^{1}H, using tetramethylsilane as an internal standard. UV–visible absorbance spectra were recorded on a UV 8453 spectrometer (Agilent, U.S.A.). Elemental analyses were performed with a Vario ELIII instrument (Elementar, Germany). MS spectra were recorded on an AXIMA-CFR™ plus MALDI-TOF-mass spectrometer (Kratos Analytical, U.K.). Pictures of the LB plates were captured by a 650D single lens reflex camera (Cannon, Japan). Binding studies based on surface plasmon resonance (SPR) phenomenon were processed on a two-channel Reichert SR7500DC optical biosensor instrument (Ametek Technologies, U.S.A.). Au sensor chips were obtained from the Reichert Company.

2.2. Synthetic procedure (Schemes 1 and 2)

2.2.1. Synthesis of 5,10,15,20-tetrakis(para-nitrophenyl) porphyrin [25]

In a 250 mL three-neck round bottomed flask, a solution of *p*-nitrobenzaldehyde (7.56 g, 0.05 mol) in propionic acid (80 mL) was

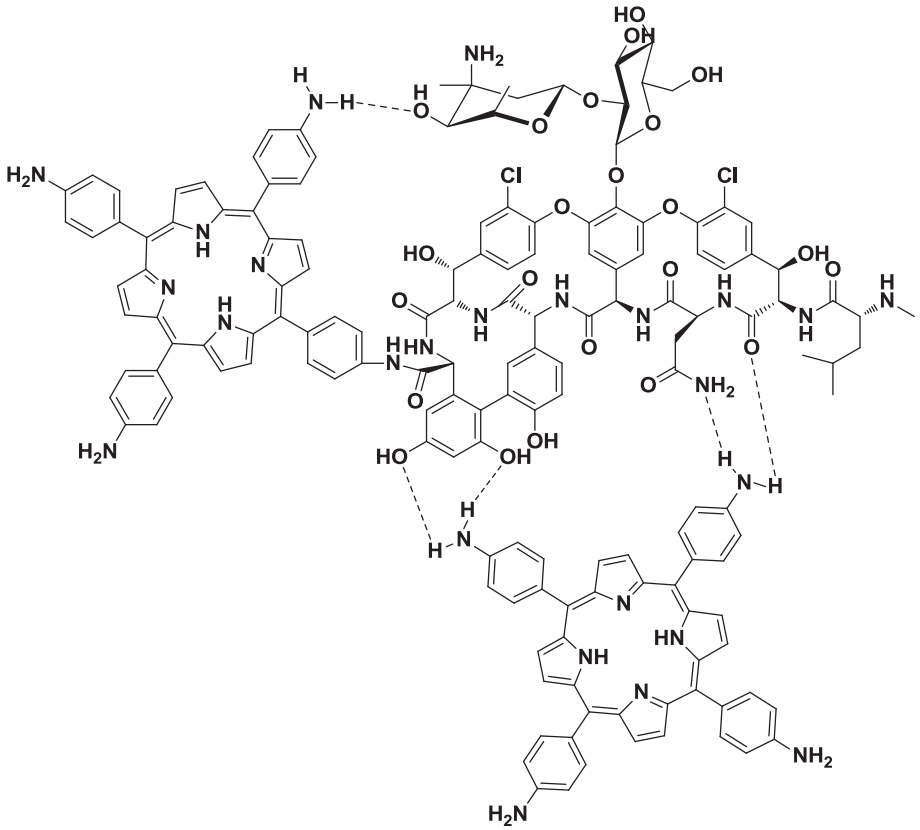

Fig. 2. Structure of conjugate porphyrin-vancomycin.

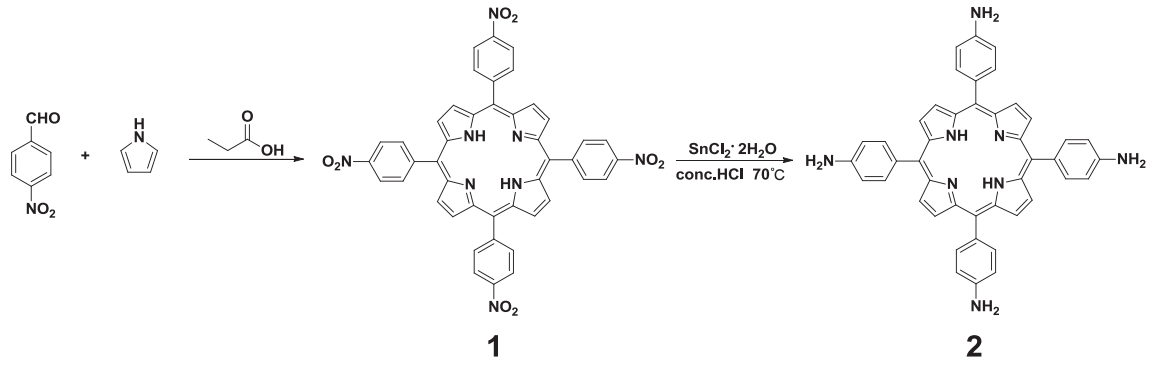

Scheme 1. Synthetic route of H_2(*p*-NH_2)TPP.

brought to 80 °C. Freshly distilled pyrrole (3.46 mL, 0.05 mol) dissolved in propionic acid (20 mL) was added drop wise, and the reaction was allowed to proceed for 20 min in the dark. The solution was heated to reflux and kept stirring for another 20 min in the dark. Then, the mixture was transferred to a 250-mL beaker, cooled to room temperature, and stored in a refrigerator for 24 h. The resulting black solid was collected by filtration, washed with H_2O repeatedly (3 × 80 mL) and dried in vacuo at 40 °C for 1.5 h. Raw

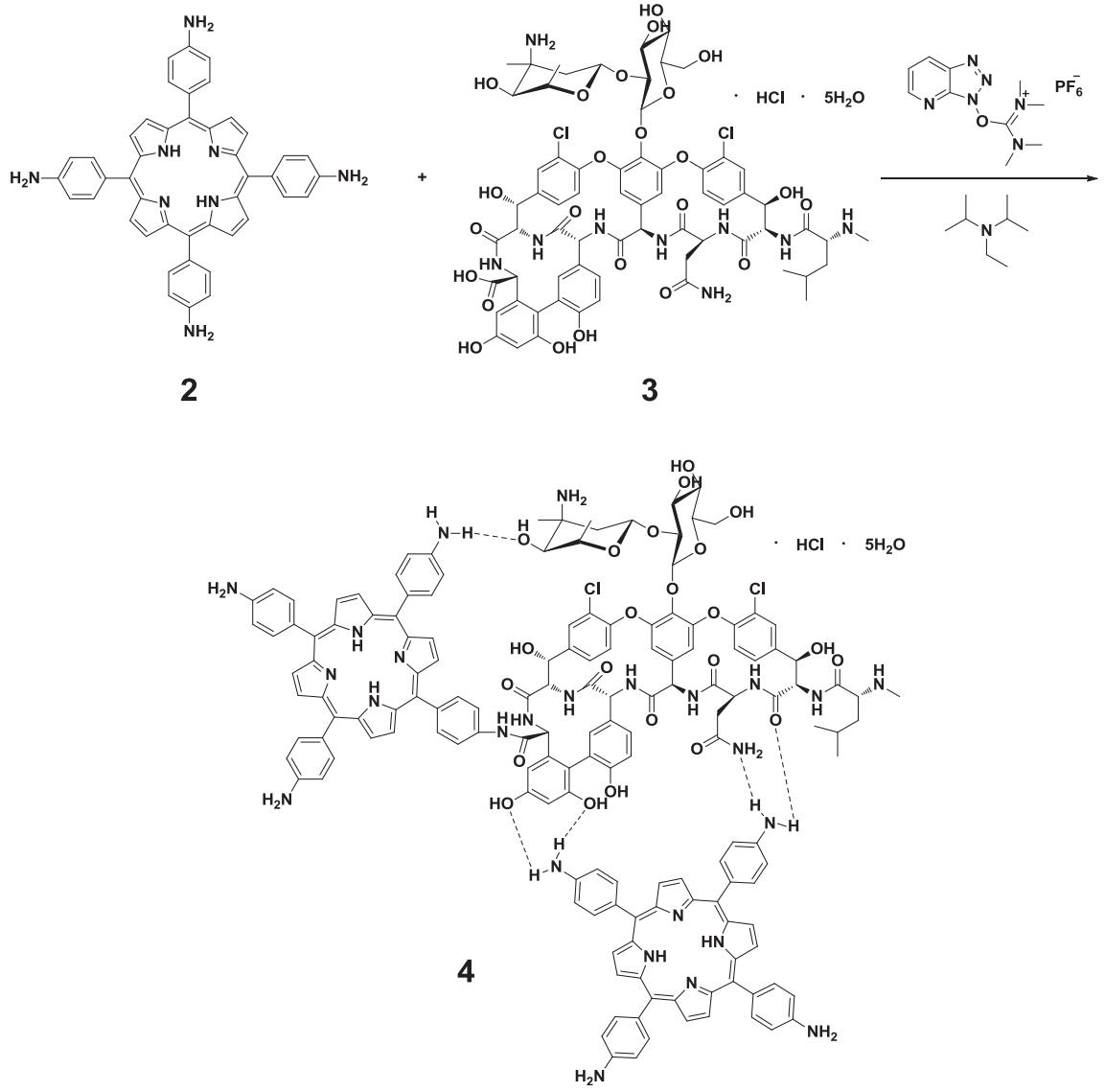

Scheme 2. Synthetic route of conjugate porphyrin-vancomycin.

product was taken up by pyridine (80 mL) in a 250 mL round bottomed flask and refluxed with stirring for an hour. The solution was allowed to cool and stand for 24 h at 0 °C. The mixture was filtered, and the collected solid was washed with acetone until the rinsings were colourless. The dark purple product was dried in vacuo at room temperature to give 1.285 g H_2(*p*-NO_2)TPP (**1**) with a total yield around 12.9%. The product was used for the next reaction directly without further purification.

Elemental analysis: $C_{44}H_{26}N_8O_8$, calcd. C, 66.50; H, 3.30; N, 14.10% found: C, 64.39; H, 2.68; N, 12.61%.

2.2.2. Synthesis of 5,10,15,20-tetrakis(para-aminophenyl) porphyrin [26]

An amount of 700 mg H_2(*p*-NO_2)TPP (0.88 mmol) was dissolved in concentrated HCl (80 mL) in a 250 mL three-neck round bottomed flask. A solution of $SnCl_2 \cdot 2H_2O$ (5.96 g, 26.4 mmol) in concentrated HCl (20 mL) was added to the reaction system. The solution was brought to 70 °C in a water bath and kept stirring for 7 h. The hot-water bath was removed and replaced by a cold-water bath and then an ice-water bath. The reaction mixture was neutralized with concentrated NaOH to a pH approximately 7.0. During this course, the resulting solution gradually changed from a deep green solution to a drab suspension. The resultant basic solution was filtered, and the greenish solid was washed twice with water, dried in vacuo at room temperature and then Soxhlet extracted with acetone. The solvent was removed under reduced pressure to give 520 mg isolated H_2(*p*-NH_2)TPP (**2**) as a purple crystal with a yield of 87.6%.

NMR: ^{1}H NMR (400 MHz, $CDCl_3$, 298 K) δ (ppm) 8.88 (s, 8H); 7.98 (d, J = 7.9 Hz, 8H); 7.06 (d, J = 7.4 Hz, 8H); 4.01 (s, 8H); -2.74 (s, 2H).

MALDI-TOF-MS (molecular ion, *m/z*): obsd. 674.8339 M^+, calcd. 674.2906 (M = $C_{44}H_{34}N_8$).

UV–vis (acetone, λ_{max}, nm): Soret band: 346–445, Q band: 495, 525, 567, 660.

Elemental analysis: $C_{44}H_{34}N_8$, calcd. C, 78.32; H, 5.08; N, 16.61% found: C, 78.29; H, 4.96; N, 16.75%.

2.2.3. Synthesis and purification of 5,10,15,20-tetrakis(para-aminophenyl) porphyrin vancomycin conjugate

In a 50 mL round bottomed flask, H_2(*p*-NH_2)TPP (33.74 mg, 0.05 mmol) and vancomycin hydrochloride (**3**) (315.16 mg, 0.2 mmol) were dissolved in 5 mL freshly distilled dimethyl sulfoxide (DMSO). The mixture was cooled to 0 °C with stirring, and *o*-(7-azabenzotriazol-1-yl)-N,N,N′,N′-tetramethyluronium hexafluorophosphate (HATU) (57.03 mg, 0.15 mmol) dissolved in 2 mL dry N,N-dimethylformamide (DMF) was added, followed by N,N-diisopropylethylamine (DIEA) (175 μL, 1 mmol). The solution was left to stand for 30 min at 0 °C with stirring, brought to room temperature and stirred for 20 h. The reaction was quenched by adding 20 mL of acetone. A deep brown solid precipitated, was filtered out, and was washed by 5 mL acetone. The crude product was dried in vacuo at room temperature to give 175 mg brown solid, which was not soluble in common organic solvent. The solid was suspended in 1 mL H_2O, and the pH was adjusted using 0.5% NaOH until the mixture became a clear yellow solution (pH approximately 8.0). After centrifugation (8000 rpm, 15 min), the supernatant was loaded onto a Sephadex G-25 column (250 × 3.0 mm), and a 0.5% NaOH solution was employed as the mobile phase at a flow rate of 1.0 mL/min. Fractions were collected every 2 mL per tube and detected by UV–visible spectrometer simultaneously to gather the targeted eluent. Identified fractions were neutralized with 1 M HCl. Precipitates were collected by centrifugation (11,000 rpm, 15 min) and dried in vacuo at room temperature to obtain 16 mg H_2(*p*-NH_2)TPP-Van conjugate (**4**) as a yellowish-green solid with a yield of 22.0%.

MALDI-TOF-MS (molecular ion, *m/z*): obsd. 2904.8615 $[M]^+$, calcd. 2904.0304 (M = $C_{154}H_{152}Cl_3N_{25}O_{28}$).

UV–vis (acetone, λ_{max}, nm): 280, 428, 525, 567, 660.

Elemental analysis: $C_{154}H_{152}Cl_3N_{25}O_{28}$ calcd. C, 63.62; H, 5.27; N, 12.04% found: C, 62.53; H, 4.92; N, 11.85%.

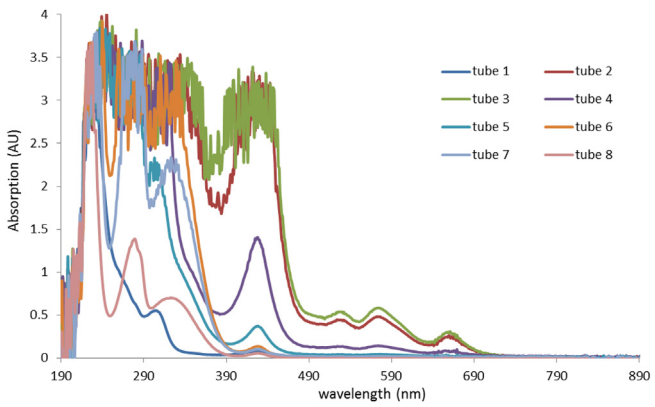

Fig. 3. UV–vis absorption spectra in monitoring the purification of conjugate **4**.

2.3. Minimum inhibitory concentration determination

The in vitro antibacterial activity of **4** was investigated by determining the MIC values against *S. aureus*, MRSA-1, MRSA-2, *E. faecalis*, VRE and *B. subtilis* strains in the dark. The MIC value determination was conducted by the Clinical and Laboratory Standards Institute (CLSI) macrodilution (tube) broth method [27].

Briefly, a single colony of the above bacteria on solid LB-agar plates was transferred to 10 mL of MH culture medium. The cultures were grown at 35 °C for 3–5 h to obtain 10^8 colony-forming units (CFU)/mL bacterium cultures according to Maxwell turbidimetry. Compounds **2**, **3** and **4** were dissolved in ddH_2O to prepare 1280 mg/L stock solutions (to obtain a clear solution, the pH of **4** was adjusted to 7.80 by NaOH, and **2** was adjusted to 6.72 by HCl). The stock solutions were diluted to 1 mL by MH medium to offer concentration series with 256, 128, 64, 32, 16, 8, 4, 2, 1, 0.5, and 0.25 mg/L, respectively. The 1 mL portion of bacterial culture (~10^6 CFU/mL) in MH medium was added sequentially into the prepared solutions. Mixtures were incubated at 37 °C for 24 h and kept away from light.

2.4. Photodynamic inactivation evaluation

Photodynamic inactivation was investigated by a traditional surface plating method [20,28,29]. In addition to *E. coli*, the same bacteria used in the MIC determination were employed.

A single colony of bacteria on LB-agar plates was transferred to 10 mL of LB culture medium and was grown at 37 °C overnight. Cells were collected by centrifugation (4 °C, 4000 rpm, 10 min), washed 3–6 times with phosphate-buffered saline (PBS) buffer (pH 7.4), and diluted with the same buffer to an $O.D._{600}$ of 0.5. Concentration series of **2**, **3**, and **4** dissolved samples with 2, 4, 6, 8, 10, and 12 μM were prepared. A 0.5 mL portion of the samples was added into 0.5 mL diluted bacterium fluid, and co-cultures were incubated in the dark at 37 °C for 30 min with shaking. All samples were illuminated for 5 min with light (400–800 nm, 350 mW/cm^2), which was produced by a xenon lamp. For each compound, paralleled experiments were conducted. Furthermore, the light dose-dependent photoinactivation of each compound with 10 μM was tested. The illumination time ranged from 0 to 10 min, respectively.

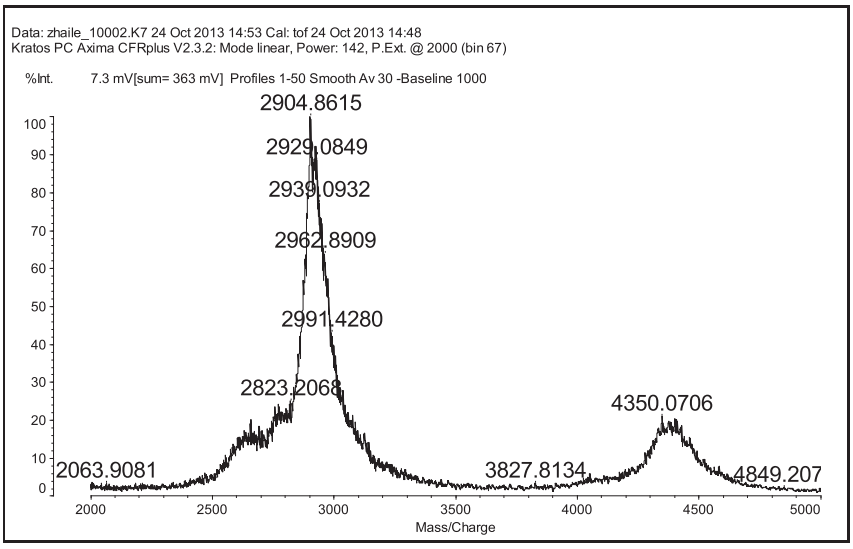

Fig. 4. MALDI-TOF mass spectrum of conjugate **4**.

Table 1
MIC values of compound **2, 3** and **4** against six bacterial strains.

Organisms	MIC (mg/L)		
	4[α]	Vancomycin(3)	H_2(*p*-NH_2)TPP(2)[α]
S. aureus	16	2	>128
MRSA-1	32	2	>128
MRSA-2	>128	32	>128
E. faecalis	>128	>128	>128
VRE	>128	>128	>128
B. subtilis	64	0.5	>128

α: MIC tests of **2** and **4** were carried out in dark.

After the photo-illuminated samples were centrifuged (4 °C, 4000 rpm, 10 min), the supernatant was removed. The bacterial pellet was resuspended and serially diluted 10^3-fold in PBS buffer. A 10 μL portion of the diluted bacterial cells (~10^4 CFU/mL) was spread on an LB-agar plate, incubated at 37 °C overnight, and the colony-forming units were counted. The percentage of bacterial mortality was quantified by dividing the number of CFUs between the tested compounds and the controls without any compounds or light exposure treatments.

2.5. Surface plasmon resonance analysis

2.5.1. Principle

SPR occurs when light incident on a metal film couples to the oscillations of the conducting electrons, plasmons, at the metal surface. Biomolecular binding events can cause changes in the refractive index close to the surface layer of an Au sensor chip. When resonance occurs, the intensity of the reflected light decreases at a sharply defined angle of incidence, the SPR angle, which is dependent on the refractive index penetrable by the evanescent wave close to the metal surface. If the SPR angle shift is monitored over time, a gradual increase of material at the surface will cause a successive increase of the SPR angle, which is detected as a shift of the position of the light intensity minimum on the diode array, and the output is the resonance signal. For a decade, research groups have applied SPR technology to study biomolecular binding events, such as antibody interactions with viruses [30–33] and small molecule interactions with DNA [34,35]. Despite the wide use of SPR phenomena in biological science, its use for the quantitative study of interactions between chemical molecules and entire living cells remains limited. In the beginning of our SPR analysis, cells were immobilized over an Au sensor chip. The samples were injected and floated over the cell layer in a precisely controlled flow. Binding analysis was monitored by the increase of the SPR signal and was outputted as a sensorgram. After the unbonded compounds were washed off by a continuous flow of buffer, the remaining signal reflected the intensity of the interaction between the compounds and cells.

2.5.2. Procedure

Series samples of **3** and **4** at 80, 40, and 20 mM were prepared as previously described. A single colony of *S. aureus* (Gram-positive)/*E.coli* (Gram-negative) on LB-agar plates was transferred to 10 mL LB culture medium and was incubated at 37 °C with shaking. Cells were harvested by centrifugation (4 °C, 4000 rpm, 10 min), were washed 3–6 times with PBS buffer, and were diluted to an $O.D._{600}$ of 0.05. Before the experiment started, the surface of the Au sensor chip was cleaned with solution of concentrated H_2SO_4 and 33% H_2O_2 in a 3:1 ratio. Disposed chips were immersed in absolute ethanol for 10 min to remove the oxide layer. SPR analysis was conducted at 25 °C. A 600 μL portion of bacterial cells sample was injected onto the chip surface for 60 min at a flow rate of 10 μL/min. After injection, the sensor chip was loaded with PBS buffer for 20 min over the two channels to reach equilibrium. Binding analysis was performed with independent injections (150 μL) of analyte samples over the immobilized cells surface in different channels repeatedly. The injections lasted 15 min and were followed by loading with PBS buffer for 10 min at the same flow rate. The process of interaction was monitored by the changes of the μRIU signal.

3. Results and discussion

3.1. Synthesis and spectral characterization of *4*

To synthesize **3**, intermediate H_2(*p*-NO_2)TPP was prepared by condensation of *p*-nitrobenzaldehyde with pyrrole in propionic acid under refluxing conditions. Having the nitro group at the *para*-position on the phenyl ring made the porphyrin insoluble in most common organic solvents; therefore, the impurities can be sufficiently removed by hot pyridine. The nitro groups were reduced with Sn (II) in an acidic medium, as illustrated in Scheme 1. The

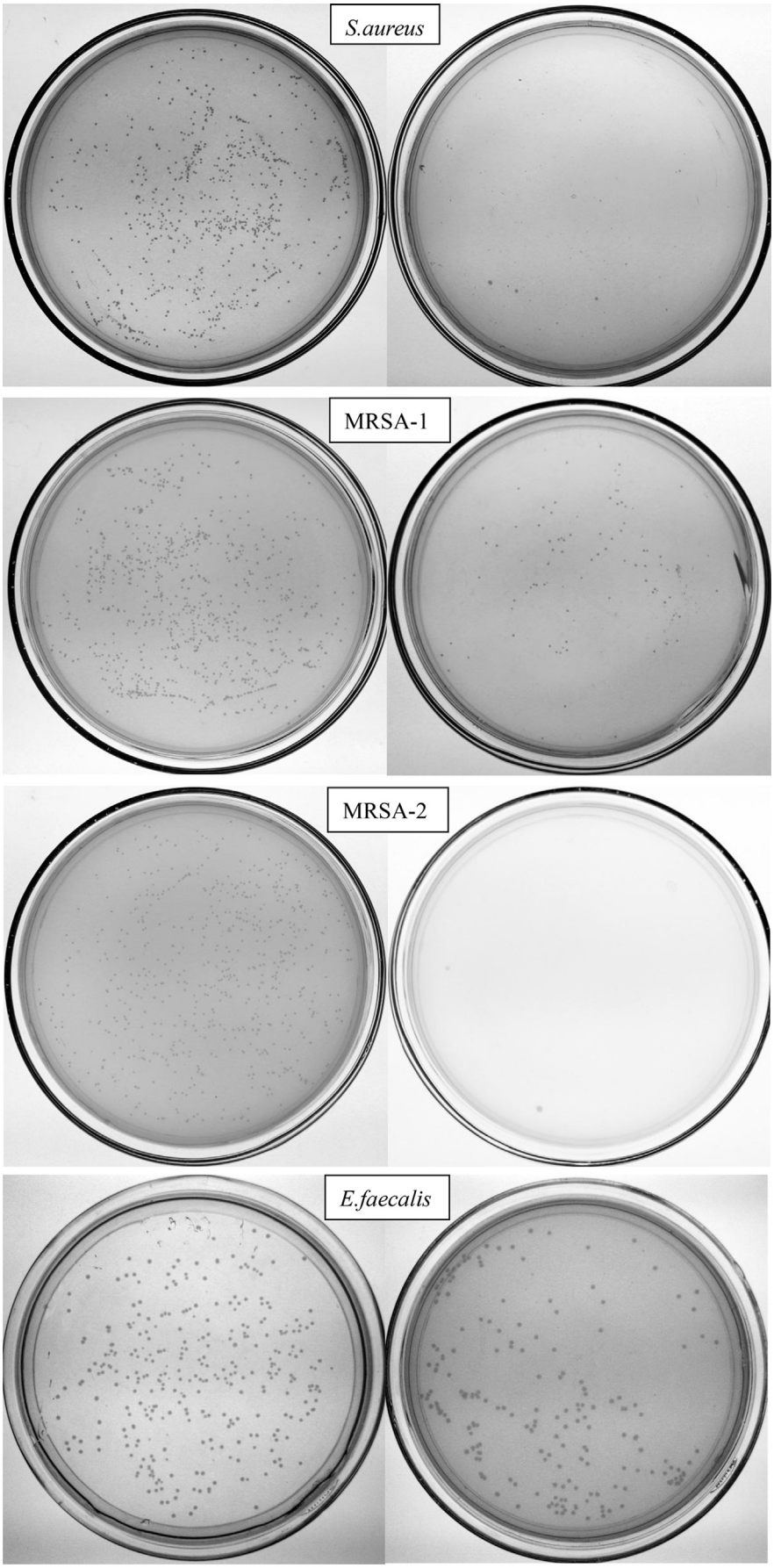

Fig. 5. CFUs comparison photographs of tested different bacterial strains on LB-agar plate. Left: CFUs control without photosensitizer in dark. Right: CFUs of suspension incubated with **4** (10 μM) under light irradiation for 5 min.

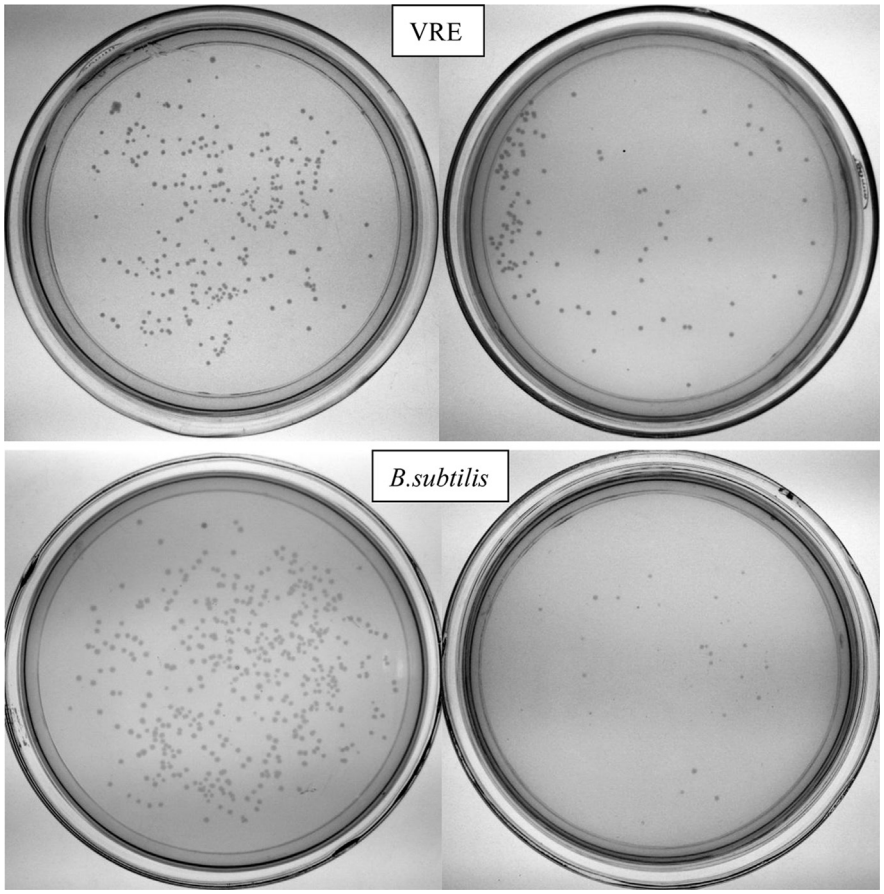

Fig. 5. (*continued*).

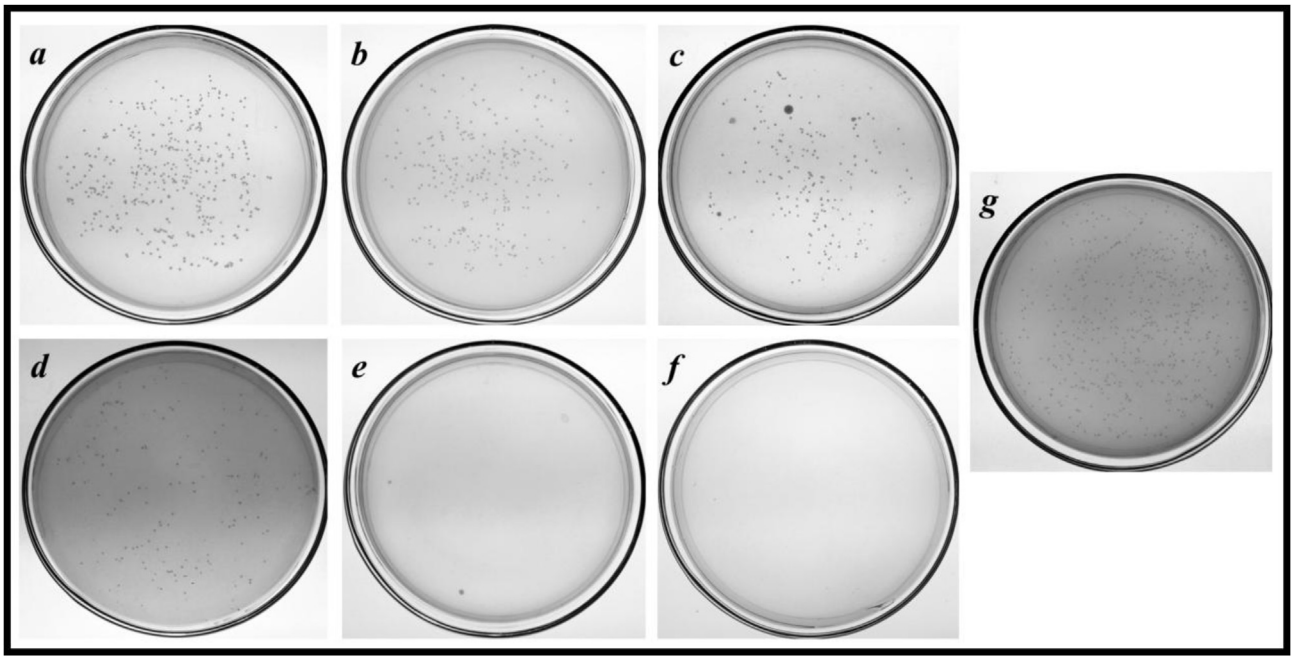

Fig. 6. Comparison photograph series of MRSA-2 CFUs on LB-agar plate with gradient concentrations of **4** after light irradiation for 5 min. The concentrations of conjugate **4**: 2 μM (a), 4 μM (b), 6 μM (c), 8 μM (d), 10 μM (e), 12 μM (f) and control (g).

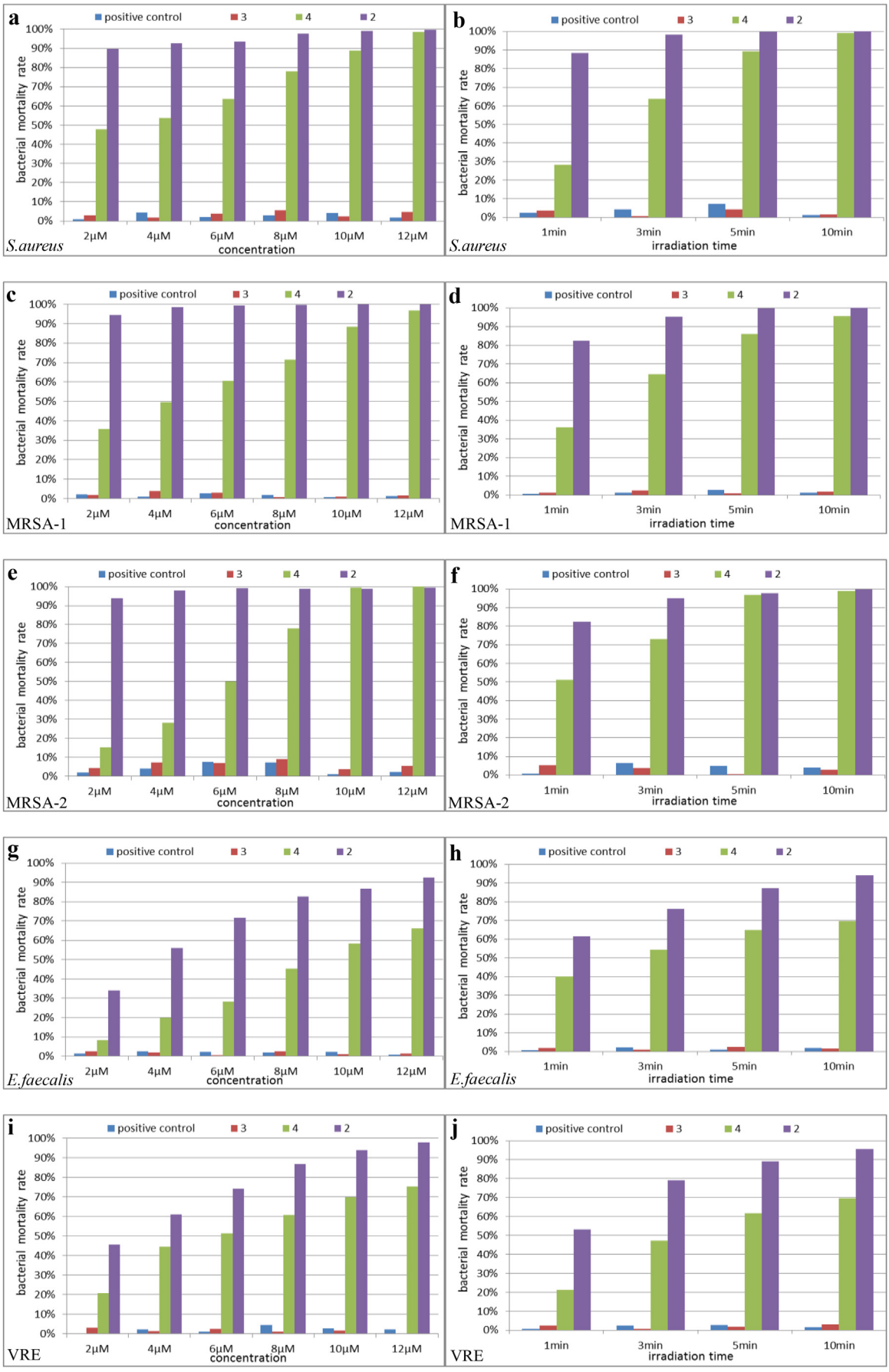

Fig. 7. Bacterial mortality rate of 6 tested bacterial strains in different concentrations of compounds and different irradiation time. (a), (c) (e), (g), (i) and (k): the irradiation time was 5 min. Bacteria treated with compounds but no light irradiation as positive control. (b), (d), (f), (h), (j) and (l): the concentrations of the compounds were 10 μM. Bacteria treated with light irradiation but no compound treatment as positive control.

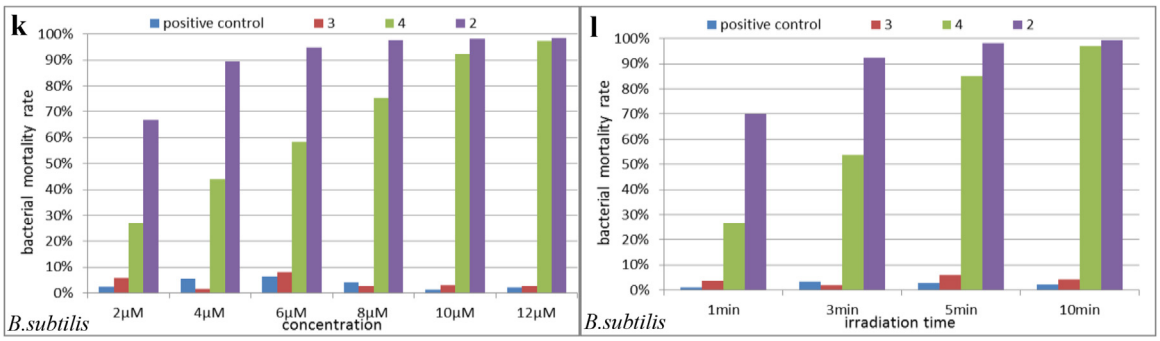

Fig. 7. (*continued*).

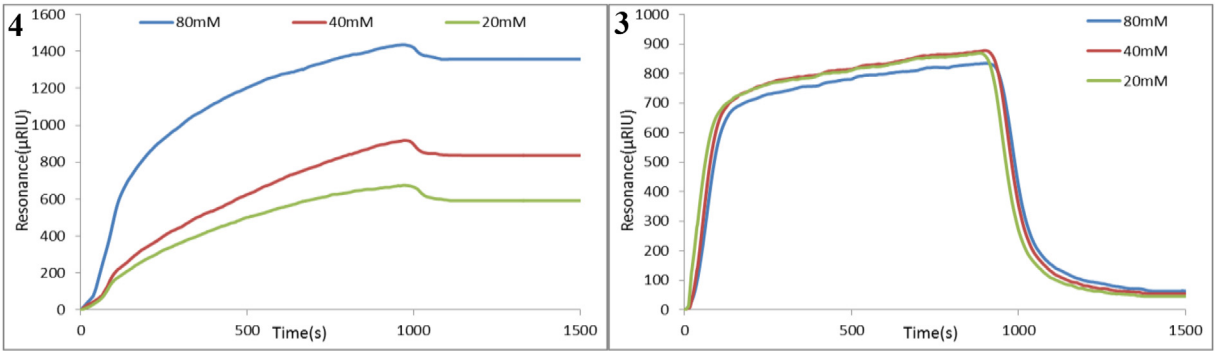

Fig. 8. SPR sensorgrams (μRIU, versus time) of different compounds binding to *S. aureus* cells.

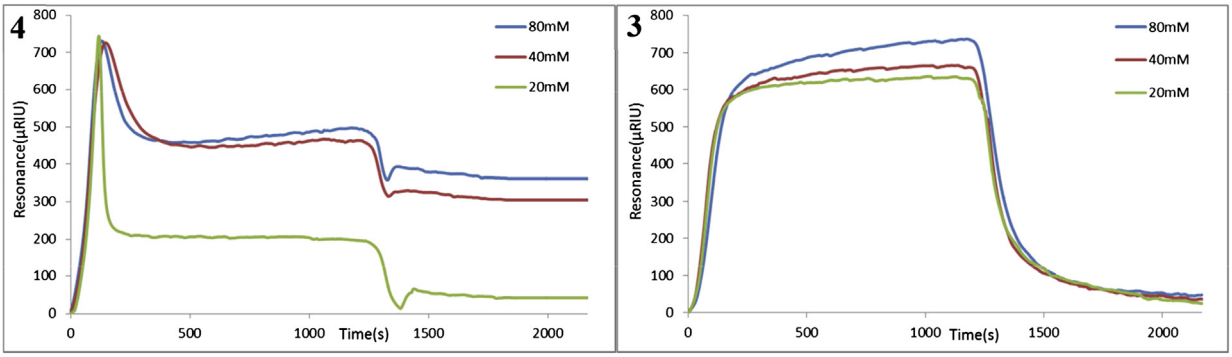

Fig. 9. SPR sensorgrams (μRIU, versus time) of different compounds binding to *E. coli* cells.

resultant H_2(*p*-NH_2)TPP had higher solubility in acetone than the nitro-substituted precursors and was obtained in 87.5% yield. To afford Van carboxamide, HATU was employed as the coupling reagent. In the subsequent purification procedure, by judging the characteristic UV–visible absorbance of the parent moieties at 280 (λ_{max} of **3**), 428, 525, 567 and 660 nm (λ_{max} of **2**, B band approximately 400 nm, Q bands between 500 and 680 nm) [36,37], purified **4** was identified and collected. As shown in Fig. 3, the obvious UV–visible absorption jumping from tube 1 to tube 2 at the above wavelength gave the harvest signal of the target molecules. Along with the elution, the absorption intensity of **4** declined; meanwhile, the peak positions remained stable from tube 3 to tube 5. From tube 6, the UV–visible absorption of the porphyrin moiety was lost, and absorption of the Van moiety climbed to a high level, which meant the unreacted Van had been eluted. The identified fractions were combined and neutralized with HCl. The precipitates were collected by centrifugation. After drying in vacuo at room temperature, the compound was confirmed by the MALDI-TOF-mass spectrum. The peak at *m/z* 2904.8615 $[M]^+$ corresponding to **4** was clearly observed, as shown in Fig. 4. While the small bread peak around *m/z* 4350, speculating to be a dimer of Van and **4**.

3.2. Minimum inhibitory concentration determination

The in vitro antibacterial activities were investigated by standard broth microdilution assays. The results of **4**, comparing its two synthetic sources against bacteria, are listed in Table 1. The conjugate showed effective antibacterial activity against *S. aureus*, MRSA-1 and *B. subtilis*, which was similar to the parent Van molecule. However, a significant MIC value decrease was also observed. The suppositional mechanism of the low activity was caused by hydrogen-bond occupation of the second H_2(*p*-NH_2)TPP molecule at the binding affinity position of Van (see Fig. 2). This position was initially employed by Van to combine with the C-terminal L-Lys-D-

Table 2
Numerical ΔμRIU values of **3** and **4** with different bacterial cells.

Concentrations (mM)	ΔμRIU			
	4		3	
	S. aureus	*E. coli*	*S. aureus*	*E. coli*
80	1358.14	361.61	63.78	47.29
40	837.29	305.07	54.77	35.90
20	591.75	41.81	46.01	24.55

Ala-D-Ala motif of Gram-positive bacterial cells to display antimicrobial activity. Nonetheless, **4** exhibited limited activity compared to Van without specific wavelength illumination.

3.3. Photodynamic inactivation evaluation

To further explore the photodynamic inactivation properties of the conjugate towards bacteria, bacterial survival experiments were performed by a traditional surface plating approach. Compound **3** and PS including **2** and **4** were treated with six bacteria strains, separately (Figs. 5 and 6). Colony counting showed that the killing efficiencies of the bacteria suspension incubated with **2** and **4** ([**2**] = [**4**] = 10 μM) under irradiation were all above 80%, except the *E. faecalis* and VRE strains, whereas the killing efficiencies for **3** were below 5%. Fig. 7 displays the bacterial mortality rate under different concentrations and irradiation times. In the control experiments, less than 10% bacterial lethality was obtained for compounds alone in the dark or only with light exposure. Among the three compounds used, **4** showed an overall photodynamic inactivation activity towards Gram-positive bacterial strains upon 5 min of specific light exposure. For the *S. aureus*, MRSA-1, MRSA-2 and *B. subtilis* strains, bacterial lethality of more than 95% at 12 μM was observed (Fig. 7: (a), (c), (e), and (k)), whereas, smaller killing efficiencies (60~70%) were detected for the most troublesome *E. faecalis* and VRE strains at the same conditions (Fig. 7: (g) and (i)). Increasing the concentrations of PS enhanced the bacterial killing efficiency for all tested bacteria. Predictably, there was no bacterial lethality detected for **3** incubated with bacterial strains upon light exposure. The photodynamic inactivation of bacteria was further investigated in the presence of different doses of white light (Fig. 7: (b), (d), (f), (h), (j) and (l)) while maintaining a fixed concentration (10 μM) of PS. The data revealed that the energy density of illumination was positively correlated to the photoinactivation. Along with the extension of the irradiation time, the bacterial lethality increased. The most significant bacterial reduction (e.g., >97% except for the *E. faecalis* and VRE strains) was achieved when 10 min of irradiation was applied. Although H_2(*p*-NH_2)TPP exhibited an emphatic lethality even at low concentration or with a short irradiation time, a lack of specificity made it inappropriate for use as a phototherapeutic reagent. Moreover, the photodynamic inactivation towards Gram-negative bacteria *E. coli* was also performed with different compound concentrations (data not shown). Similarly, **2** displayed the highest photoinactivation potency against *E. coli* among the three compounds. However, there was almost no lethality observed in *E. coli* treatments with **4**, which was similar to the behaviour of the parent Van molecule in the in vitro antibacterial activity test. The results unequivocally demonstrated that Van acted as an efficient affinity ligand and aided in targeting and accumulating the porphyrin moiety in the Gram-positive bacterial cells. Irradiated photosensitizer **4** was able to generate sufficient quantities of cytotoxic oxygen species, which diffuse into and affect the growth of the strains, resulting in cell destruction without causing damage to the neutral cells.

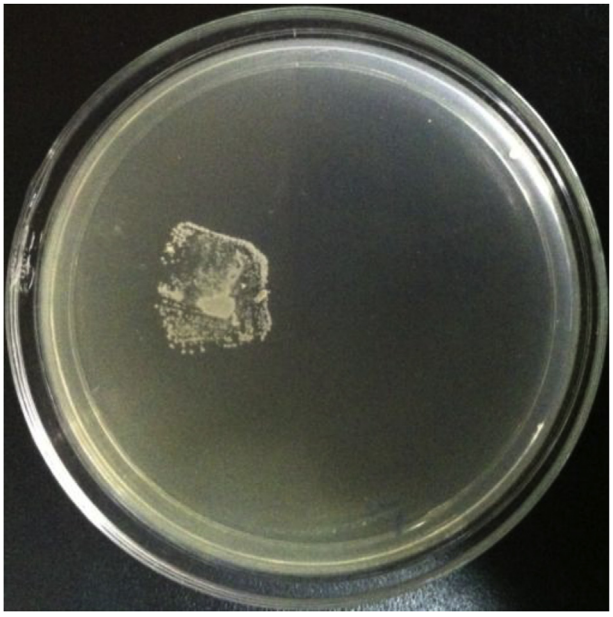

Fig. 10. Photograph of *S. aureus*-loaded Au chip after incubation.

3.4. Surface plasmon resonance analysis

The binding affinity of **4** towards bacterial cells was identified by SPR. In a typical study, the Gram-positive bacteria, *S. aureus*, and the Gram-negative bacteria, *E. coli*, were chosen as model organisms. The monitored signals of μRIU reflecting the formation of a bacterial cell layer at the chip surface were stable and repeatable. After the layer of cells was formed, a flow of **3**/**4** passed the sensor surface, and the signal began to rise. The detected sensorgrams demonstrated the combination process between cells and **3**/**4** are illustrated in Figs. 8 and 9. To gain a better understanding of the sensorgrams, the numerical ΔμRIU values are presented in Table 2. As shown, **4** exhibited an excellent combining capacity toward *S. aureus* vs *E. coli*, with a value approximately 14 times larger at the concentration of 20 mM. The disparity was mainly caused by the high affinity to *S. aureus* cells of the Van moiety. The reason for the distinct differences between **3** and **4** toward *S. aureus* cells is still unclear, and the research is underway. Nevertheless, it should be noted that after linking to Van, the selectivity of H_2(*p*-NH_2)TPP against the two types of bacterial cells was effectively improved, which overcomes the disadvantage of common PS. Moreover, the SPR data also expounded the photoinactivation results precisely: for little combination of **4** with Gram-negative *E. coli* cells, no photodynamic inactivation was observed. In addition, after all analysis was completed, the used Au chip was transferred to an LB-agar plate and incubated at 37 °C overnight. Fig. 10 shows that bacterial cells survived throughout the assay, which meant the real time process of SPR data were obtained on living cells.

4. Conclusions

In summary, this work presents a simple and novel phototherapeutic reagent by conjugating the photosensitizer H_2(*p*-NH_2)TPP with a Van moiety. The conjugate was synthesized by three simple steps, isolated using a gel molecular sieve purification technique, characterized by UV–visible spectroscopy, and confirmed by the MALDI-TOF mass spectrum. Based on the MIC data, the conjugate shows a certain degree of antimicrobial activity in vitro. Further SPR analysis with living bacterial cells

demonstrates that the selectivity of porphyrin was successfully improved by linking to the Van ligand. On the other hand, the conjugate exhibits a relatively higher binding affinity to Gram-positive bacterial cells and retains potent photodynamic inactivation activity against antibiotic resistant pathogens compared to the synthetic sources alone. The most crucial conclusion is that the conjugate displays overall photodynamic inactivation activity towards six Gram-positive bacterial strains upon 5 min (10 μM) of light exposure, with a killing efficiency from 60% to 95%. Overall, the constructed conjugation can be used to identify Gram-positive bacteria and generate singlet oxygen effectively under white light irradiation, which overcomes the challenges of common PS. In this regard, we expect that the skeleton and data gained in this work can provide a starting point for the exploration of alternative options for fighting against antibiotic resistant bacterial infections.

Acknowledgements and funding

We are grateful for assistance in the photodynamic studies from Dr. Dan Sun at the Laboratory of Photonics and Photon Technique at Northwest University. This work was supported by grants 21272186 and 81361138018 (to K.W.Y.) from the National Natural Science Fund of China and key grant 2014KW23-03(to K.W.Y.) for International Cooperation of Shaanxi Province. We also acknowledge the financial support from The Graduate Student Innovation Fund from Northwest University (YZZ12033).

References

[1] Barna JC, Williams DH. The structure and mode of action of glycopeptide antibiotics of the vancomycin group. Ann Rev Microbiol 1984;38:339–57.
[2] Reynolds PE. Structure, biochemistry and mechanism of action of glycopeptide antibiotics. Eur J Clin Microbiol Infect Dis 1989;8:943–50.
[3] Kahne D, Leimkuhler C, Lu W, Walsh C. Glycopeptide and lipoglycopeptide antibiotics. Chem Rev 2005;105:425–48.
[4] Walsh CT. Vancomycin resistance: decoding the molecular logic. Science 1993;261:308–9.
[5] Arthur M, Courvalin P. Genetics and mechanisms of glycopeptide resistance in enterococci. Antimicrob Agents Chemother 1993;37:1563–71.
[6] Arthur M, Depardieu F, Reynolds P, Courvalin P. Quantitative analysis of the metabolism of soluble cytoplasmic peptidoglycan precursors of glycopeptide-resistant enterococci. Mol Microbiol 1996;21:33–44.
[7] Healy VL, Lessard IA, Roper DI, Knox JR, Walsh CT. Vancomycin resistance in enterococci: reprogramming of the D-Ala-D-Ala ligases in bacterial peptidoglycan biosynthesis. Chem Biol 2000;7:109–19.
[8] Li L, Xu B. Multivalent vancomycins and related antibiotics against infectious diseases. Curr Pharm Des 2005;11:3111–24.
[9] Xing B, Jiang T, Wu X, Liew R, Zhou J, Zhang D, et al. Molecular interactions between glycopeptide vancomycin and bacterial cell wall peptide analogues. Chemistry 2011;17:14170–7.
[10] Williams DH, Maguire AJ, Tsuzuki W, Westwell MS. An analysis of the origins of a cooperative binding energy of dimerization. Science 1998;280:711–4.
[11] Loll PJ, Axelsen PH. The structural biology of molecular recognition by vancomycin. Annu Rev Biophys Biomol Struct 2000;29:265–89.
[12] Henderson BW, Dougherty TJ. How does photodynamic therapy work? Photochem Photobiol 1992;55:145–57.
[13] Dolmans DE, Fukumura D, Jain RK. Photodynamic therapy for cancer. Nat Rev Cancer 2003;3:380–7.
[14] Celli JP, Spring BQ, Rizvi I, Evans CL, Samkoe KS, Verma S, et al. Imaging and photodynamic therapy: mechanisms, monitoring, and optimization. Chem Rev 2010;110:2795–838.
[15] Castano AP, Mroz P, Hamblin MR. Photodynamic therapy and anti-tumour immunity. Nat Rev Cancer 2006;6:535–45.
[16] Maisch T, Szeimies RM, Jori G, Abels C. Antibacterial photodynamic therapy in dermatology. Photochem Photobiol Sci 2004;3:907–17.
[17] Demidova TN, Hamblin MR. Photodynamic therapy targeted to pathogens. Int J Immunopathol Pharmacol 2004;17:245–54.
[18] Xing B, Jiang T, Bi W, Yang Y, Li L, Ma M, et al. Multifunctional divalent vancomycin: the fluorescent imaging and photodynamic antimicrobial properties for drug resistant bacteria. Chem Commun 2011;47:1601–3.
[19] Strassert CA, Otter M, Albuquerque RQ, Höne A, Vida Y, Maier B, et al. Photoactive hybrid nanomaterial for targeting, labeling, and killing antibiotic-resistant bacteria. Angew Chem Int Ed Engl 2009;48:7928–31.
[20] Xing C, Xu Q, Tang H, Liu L, Wang S. Conjugated polymer/porphyrin complexes for efficient energy transfer and improving light-activated antibacterial activity. J Am Chem Soc 2009;131:13117–24.
[21] Suci PA, Varpness Z, Gillitzer E, Douglas T, Young M. Targeting and photodynamic killing of a microbial pathogen using protein cage architectures functionalized with a photosensitizer. Langmuir 2007;23:12280–6.
[22] Shao Q, Xing B. Enzyme responsive luminescent ruthenium(II) cephalosporin probe for intracellular imaging and photoinactivation of antibiotics resistant bacteria. Chem Commun 2012;48:1739–41.
[23] Lovell JF, Chan MW, Qi Q, Chen J, Zheng G. Porphyrin FRET acceptors for apoptosis induction and monitoring. J Am Chem Soc 2011;133:18580–2.
[24] Cormick MP, Alvarez MG, Rovera M, Durantini EN. Photodynamic inactivation of Candida albicans sensitized by tri- and tetra-cationic porphyrin derivatives. Eur J Med Chem 2009;44:1592–9.
[25] Bettelheim A, White BA, Raybuck SA, Murray RW. Electrochemical polymerization of amino-, pyrrole-, and hydroxy-substituted tetraphenylporphyrins. Inorg Chem 1987;26:1009–17.
[26] Guo Z, Mao J, Qin O, Zhu Y, He L, Xin L, et al. Noncovalent functionalization of single-walled carbon nanotube by porphyrin: dispersion of carbon nanotubes in water and formation of self-assembly donor-acceptor nanoensemble. J Dispers Sci Technol 2010;31:57–61.
[27] Wayne PA. Performance standards for antimicrobial susceptibility testing: 18th informational supplement. Clinical and Laboratory Standards Institute; 2009. M100–S19.
[28] Xiao JM, Feng L, Zhou LS, Gao HZ, Zhang YL, Yang KW. Novel fluorescent cephalosporins: synthesis, antimicrobial activity and photodynamic inactivation of antibiotic resistant bacteria. Eur J Med Chem 2013;59:150–9.
[29] Liu CC, Zhou LS, Liu JY, Xiao JM, Gao HZ, Yang KW. Photoinactivation of vancomycin-resistant enterococci and bacillus subtilis by a novel norvancomycin-rhodamine B conjugate. New J Chem 2013;37:575–80.
[30] McDermott Jr BM, Rux AH, Eisenberg RJ, Cohen GH, Racaniello VR. Two distinct binding affinities of poliovirus for its cellular receptor. J Biol Chem 2000;275:23089–96.
[31] Xing L, Tjarnlund K, Lindqvist B, Kaplan GG, Feigelstock D, Cheng RH, et al. Distinct cellular receptor interactions in poliovirus and rhinoviruses. EMBO J 2000;19:1207–16.
[32] Dubs MC, Altschuh D, Van Regenmortel MH. Interaction between viruses and monoclonal antibodies studied by surface plasmon resonance. Immunol Lett 1992;31:59–64.
[33] Chenail G, Brown NE, Shea A, Feire AL, Deng G. Real-time analysis of antibody interactions with whole enveloped human cytomegalovirus using surface plasmon resonance. Anal Biochem 2011;411:58–63.
[34] Dixon IM, Lopez F, Tejera AM, Estève JP, Blasco MA, Pratviel G, et al. A g-quadruplex ligand with 10000-fold selectivity over duplex DNA. J Am Chem Soc 2007;129:1502–3.
[35] Dixon IM, Lopez F, Estève JP, Tejera AM, Blasco MA, Pratviel G, et al. Porphyrin derivatives for telomere binding and telomerase inhibition. Chembiochem 2005;6:123–32.
[36] Zakavi S, Omidyan R, Ebrahimi L, Heidarizadi F. Substitution effects on the UV–vis and ^{1}H NMR spectra of the dications of meso and/or β substituted porphyrins with trifluoroacetic acid: electron-deficient porphyrins compared to the electron-rich ones. Inorg Chem Commun 2011;14:1827–32.
[37] Zheng W, Shan N, Yu L, Wang X. UV-visible, fluorescence and EPR properties of porphyrins and metalloporphyrins. Dyes Pigm 2008;77:153–7.